A Rulkov neuron under the influence of memristive electromagnetic radiation: Dynamic analysis and experiment through microcontroller board

Victor Kamdoum Tamba[a], Junior Tchiaze Tofou[a], Viet-Thanh Pham[b,*], and Shaher Momani[c,d]

[a] *Department of Telecommunication and Network Engineering, IUT-Fotso Victor of Bandjoun, University of Dschang, P. O. Box: 134, Bandjoun, Cameroon*

[b] *Faculty of Electronics Technology, Industrial University of Ho Chi Minh City, Ho Chi Minh City, Vietnam*

[c]*Nonlinear Dynamics Research Center (NDRC), Ajman University, Ajman 20550, United Arab Emirates*

[d]*Department of Mathematics, Faculty of Science, University of Jordan, Amman 11942, Jordan*

* *Corresponding author:* phamvietthanh@iuh.edu.vn; tel.: (+84) 915575666

Abstract

The processing and transmission of information in a biological brain is assured by the neurons, which communicate together or process information through the emission of electrical impulses (called action potential). For this reason, a potential difference occurs both between neurons and between the inner and outer membranes of an individual neuron. Due to this, the biological neural network is constantly subjected to intricate electromagnetic conditions. In this study, a non-polynomial memristor is employed to simulate the impact of electromagnetic radiation on an improved Rulkov neuron. From the theoretical investigations carried out, the system shows both stable and unstable dynamics depending on the value of one of its specific parameters. Results from numerical analyses uncover that the improved Rulkov neuron under electromagnetic radiation can exhibit rich and diversified dynamics such as self-excited and hidden attractors, evolving from regular to chaotic motions. In addition, for certain specific values of its parameters, interesting and intriguing features such as antimonotonicity (i.e. bubble like bifurcation) and offset boosting are revealed. Furthermore, physical results obtained from breadboard experiments carried out using an Arduino Due microcontroller board corroborates with numerically obtained findings. The improved Rulkov neuron is finally exploited to generate random bits and NIST test is performed to confirm the unpredictable features of the generated bits.

Keywords: Biological neural network, non-polynomial memristor, improved Rulkov neuron, offset boosting behaviors, antimonotonicity, self-excited and hidden attractors, microcontroller implementation.

1. Introduction

Neuromorphic computing marks a significant breakthrough in artificial intelligence and data handling [1-3]. This paradigm emulates the architecture and operational principles of the human brain, leveraging synthetic neurons and synapses in both physical and digital systems to manage and interpret information [4-6]. The brain is the central organ of the nervous system responsible for the sensory information integration and the transmission of motor responses [7-9]. It can manage and treat more than thousands of pieces of information in a very short length of time, which makes it the most complex structure known. One of the greatest innovations in science is the conception of artificial systems capable of mimicking the functioning of the brain [10,11]. However, given the numerous difficulties faced in the study and understanding of brain functions, most of the artificial systems developed up to now can only simulate some functions of a biological brain. Some important of these systems include the Hopfield Neural Network (HNN) [12], which because of its pronounced nonlinear characteristics and adaptability, is broadly used to model intricate dynamical patterns in the brain and more particularly those of a chaotic nature. The FitzHugh-Nagumo neuron model [13,14], that was modeled to define neuronal responsiveness and spike activity. The Rulkov neuron model [15,16], which simulates the spiking firings of a brain etc. A great variety of Artificial Neural Networks (ANN) and neuron models are found in literature, each presenting interesting behaviors and particularities on brain function. In view of ameliorating our understanding of brain functions and by analogy neurological diseases, these ANNs are continuously developed, studied and improved. Among the proposed ANNs found in literature, we have the Rulkov neuron which is a neuron model composed of a two-dimensional discrete map, capable of simulating the firing and spiking dynamics observed in biological neurons [15,16]. It is a more recent model of ANNs and because of its discrete nature, making it difficult for such a model to be used in the development of neuromorphic circuits, the model was not of much interest [17]. However, an uninterrupted formulation of the Rulkov neuron was presented in [18], whose limitations to practical engineering applications due to multiplication terms found in the model, were revised by Shaoshua and its coworkers [17] by replacing the nonlinear function with multiple expensive multipliers by a multiplier-free nonlinear function. Using a flux controlled memristor, the authors explored the dynamics of this improved Rulkov neuron model under the effects of

electromagnetic induction and external periodic stimulus. This improved Rulkov neuron being a more practically applicable model, the interest for the Rulkov neuron is seen to be renewed. Notably, important dynamics of this model such as the coexistence of chaotic and periodic firing dynamics were disclosed in [19], and the model applied to information patterns. It is known from literature that external stimuli have a great influence on the dynamics of ANNs as many of them are found to describe richer dynamics when exposed to these factors. This is rather seen for Hopfield field neural networks like in [20] where, Wan and its copartners investigated a memristive synapse weight HNN model influenced by electromagnetic induction and electromagnetic radiation, which is found to describe bistable patterns and controllable multi-scroll dynamics. Lai and Yang [21] designed a local active memristor and exploited it to study the effect of electromagnetic radiation on the dynamics of neurons. They proved that the model generates hyperchaotic behaviors and coexistence of attractors when the memristor is introduced and the intensity of the electromagnetic radiation is increased. Experimental study is pointed out to support the computational results. In [22], a dual-neuron system emerged through the interconnection of distinct Rulkov neurons using a memory element, investigating the impact of memristive electromagnetic induction. The proposed model is examined by the authors. Simulation findings demonstrated that the model under consideration generates fixed points, periodic and chaotic attractors, chaos crisis, Feigenbaum bifurcation and extreme multistability depending on the initial states of the memristor and gated ion concentration. They investigated also the phase synchronization of the two Rulkov neurons regarding the memristor coupling strength and its initial state. The numerical simulations suggested that the neurons are in phase when the memristor coupling strength and its initial condition are increased. The work is ended by performing experimental study, which validated the numerical findings. Reference [23] investigated a discrete memristive Rulkov neuron model affected by magnetic induction. The authors demonstrated that the model has complicated dynamics such as regime transition behaviors, transient chaos, bursting regimes, and hyperchaotic states. They validated the simulation findings by carrying out an experimental study. Ding with its colleagues [24] studied a Rulkov type system affected by external electromagnetic exposure. They demonstrated that the model displays many kinds of complicated dynamic behaviors. ARM-based digital circuit implementation and image encryption are carried out not only to validate the numerical simulations, but also to prove the applicability of the model. Inspired by all these works and the importance of electromagnetic radiation on dynamical behaviors of neurons, this paper is aimed at exploring the effects of electromagnetic radiation using a non-polynomial memristor on the dynamic behaviors of the improved Rulkov neuron. As contribution, this work:

- Designs a memristive improved Rulkov neuron based on a non-polynomial memristor used to emulate the effects of electromagnetic radiation.
- Studies the basic properties and bounded analysis of the elaborated memristive improved Rulkov neuron.
- Simulates numerically the elaborated model and discloses its rich and diversified dynamical patterns including self-triggered and concealed firings, adaptation amplification behavior and bubble-like bifurcation.
- Implements the introduced model onto an Arduino Due microcontroller, thereby obtaining an electronic circuit capable of reproducing the dynamics of the studied model.

The rest of this paper is organized as follows: In Section II, the memristive improved Rulkov neuron model is presented followed by the analysis of the stability of its equilibrium points and its bounded analysis. Section III outlines the dynamic behaviors of the model using numerical simulations. This is followed in Section IV by the validation of the memristive enhanced Rulkov system via a digital card. This step is essential for validating the numerical results. The application of the proposed memristive improved Rulkov neuron model to Random Number Generator is described in Section V. Section VI concludes the paper.

2. Design of the improved Rulkov neuron under electromagnetic radiation, its stability and bounded analysis

2.1. Overview of the improved Rulkov neuron incorporating a multiplier-free non-linear function

The continuous Rulkov neuron as proposed by Xu et al. [18] is expressed as follows:

$$\begin{cases} \dfrac{dx}{d\tau} = \dfrac{\alpha}{1+x^2} - x + y, \\ \dfrac{dy}{d\tau} = -\beta x - \sigma. \end{cases} \tag{1}$$

where the excitability of the neurons and signal transmission are both controlled by the positive constants α, β and σ. The continuous time version of Rulkov neuron is considered here because it can perfectly represent real-world physical phenomena. It is more flexible and has inherent mathematical elegance. In addition, it has the best correspondence with the needs and conception of integrated neuromorphic circuits contrarily to the discrete time model. The

neuronal membrane potential alongside the recovery variable of the neurons is respectively represented by the currents x and y.

The transfer function given by the nonlinear function $1/(1+x^2)$ brings difficulties in engineering application of such a model. This was corrected by Shaoshua et al. who proposed an enhanced model of the Rulkov neuron incorporating a multiplier-free nonlinear transfer function expressed as $H(x) = -\tanh\left(a|x|\right)+b$, with tunable parameters a and b used to correspond with the initial nonlinear function as shown as [17]:

$$\begin{cases} \dfrac{dx}{d\tau} = \alpha H(x) - x + y, \\ \dfrac{dy}{d\tau} = -\beta x - \sigma. \end{cases} \tag{2}$$

As a primary criterion, the minimal Root Mean Square Error (RMSE) is achieved for $a = 0.5$ and $b = 1$ when assessing the performance between the original and multiplier-free function using the RMSE, by sorting out the optimal fitting parameters [17].

2.2. Description and characterization of the non-polynomial memristor

While modeling ANNs subjected to an external factor such as electromagnetic radiation, the use of memristors is essential. This is because an electromagnetic induction current can be produced via the controlled motion of charged ions by the established electromagnetic field when a neuron is subjected to electromagnetic radiation [25]. This makes it possible for a memory component to be employed to characterize the relationship between magnetic flux and membrane potential, for which the magnetic flux across the membrane potential is considered as the effects of electromagnetic radiation [13]. In this paper, we made use of a non-polynomial memristor recently introduced and used by Yu et al. to explore the influence of electromagnetic radiation and memristive synapse weighting on a Hopfield neural network, from where controllable single and multiple direction multiscrolls are disclosed [26]. The main advantage of this memristor model is its smoothness and continuity which ensures a better stability. In addition to this, it offers a constant level of computational complexity, showing a better non-linear dynamic compared to polynomial memristors, which makes it a more accurate model closer to synaptic plasticity. According to the memristor theory, this non-polynomial memristor model is designed as expressed below [26]:

$$\begin{cases} i_m = W(x)v_m \\ W(x) = b + cf(x) \\ \dot{x} = dv_m - ef(x) \end{cases} \tag{3}$$

with the memductance represented by $W(x)$. The state variable, x, defines the internal state of the memristor while b, c, d and e are its parameters. The memristive internal state is given by $f(x)$ which can be an odd or even function having the following expressions as described in [26]:

$$f_{odd}(x) = \begin{cases} 2\pi A_m F_m x - 2\pi N_m, & x > \dfrac{N_m}{F_m} \\ A_m \sin\left(2\pi F_m x\right), & -\dfrac{N_m}{F_m} \le x \le \dfrac{N_m}{F_m} \\ 2\pi A_m F_m x + 2\pi N_m, & x < -\dfrac{N_m}{F_m} \end{cases} \tag{4}$$

for its odd form, and

$$f_{even}(x) = \begin{cases} 2\pi A_m F_m x - 2\pi\left(N_m + 0.5\right), & x > \dfrac{N_m + 0.5}{F_m} \\ -A_m \sin\left(2\pi F_m x\right), & -\dfrac{N_m + 0.5}{F_m} \le x \le \dfrac{N_m + 0.5}{F_m} \\ 2\pi A_m F_m x + 2\pi\left(N_m + 0.5\right), & x < -\dfrac{N_m + 0.5}{F_m} \end{cases} \tag{5}$$

for its even form,

with A_m, F_m and N_m describing parameters of the function. The non-polynomial memristor utilized in this study is derived from the even form of the function $f(x)$. Its characteristics are demonstrated through the visualization of its characteristic curves. This goal is achieved by exciting the memristor with a sinusoidal signal in the form $v_m = A\sin\left(2\pi ft\right)$. Parameters A and f are respectively, the amplitude and frequency of the excitation signal. Figure 1 shows the features of the memory component under consideration for fixed values of system parameters and initial conditions.

From Figures 1(a) and 1(b), it is observed that an increase in the amplitude A of the excitation signal leads to a corresponding increase in I-V characteristics. While, in Figures 1(b) and 1(b),

it is remarked that there is a decrease in I-V characteristics with increasing frequency f of the excitation signal. These figures cross the origin and describe the shape of eight, which is the signature of the memristor. As observed in Fig.1c, the memristor demonstrates non-volatility, enabling data retention even without a power supply. These results fit with the characteristics of a memristor.

3.3. The improved Rulkov neuron under electromagnetic radiation

For a clearer and easier understanding, Figure 2 presents a topology diagram of the improved Rulkov neuron model under electromagnetic radiation.

Using the non-polynomial memristor described above, the improved Rulkov neuron as presented by Eq. (2) is exposed to electromagnetic radiation, from where our improved Rulkov neuron under electromagnetic radiation is established as:

$$\begin{cases} \dot{x} = \alpha\left(-\tanh\left(0.5|x|\right)+1\right) - x + y + I_{ext} + kx\left(b + cf\left(z\right)\right) \\ \dot{y} = -\beta x - \sigma \\ \dot{z} = dx - ef\left(z\right) \end{cases} \tag{6}$$

with an external stimulus current $I_{ext} = A\sin\left(2\pi ft\right)$. The term $kx\left(b+cf\left(z\right)\right)$ is the current induced because of the memristive electromagnetic radiation, where k represents the electromagnetic induction strength.

4.4. Bounded analysis

Using the Lyapunov stability analysis method, the ability of the studied model (as expressed in Eq. 6) to perform chaotic behaviors is evaluated. From a Lyapunov function which is both positive and definite, formulated as:

$$V(x,y,z) = \frac{1}{2}(x^2 + y^2 + z^2) \tag{7}$$

where $V(x,y,z) > 0$. The time derivative is calculated as:

$$\dot{V}(x,y,z) = x\dot{x} + y\dot{y} + z\dot{z} \tag{8}$$

Substituting Eq. (6) into Eq. (8), we have

$$\dot{V}(x,y,z) = \alpha xH(x) - (1-kb)x^2 + xy - \beta xy - \sigma y + I_{ext}x - kcx^2 f(z) + dxz - ezf\left(z\right) \tag{9}$$

where $H(x) = -\tanh\left(0.5|x|\right)+1$. The cubic term $kcx^2 f(z)$ being a cubic term, it exceeds the magnitude of the quadratic term, resulting in the absence of an upper bound when z surpasses a specific threshold. To ensure the system remains bounded in this scenario, let $z \in (L_1, L_2)$ and $kcx^2 f(z) + dxz - ezf(z) \le |kc\alpha| x^2 + |d\beta x| + |e\alpha\beta|$ where α and β are respectively the maximum values of $|f(z)|$ and $|z|$. Eq. (9) thereby becomes:

$$\begin{aligned}\dot{V}(x,y,z) &= \left(\alpha H(x) + |d\beta| + I_{ext}\right)x - \left(1 - kb - |kc\alpha|\right)x^2 + xy - \beta xy - \sigma y + |e\alpha\beta| \\ &\le -\left[\left(\sqrt{\left(1-kb-|kc\alpha|\right)}x - \frac{\left(\alpha + |d\beta| + I_{ext}\right)}{2\sqrt{\left(1-kb-|kc\alpha|\right)}}\right)^2 - \left(\frac{x}{2}+y\right)^2 + \left(\frac{x}{2}+\beta y\right)^2 + \left(\frac{y}{2}+\sigma\right)^2\right] \\ &\quad + \frac{\left(\alpha + |d\beta| + I_{ext}\right)^2}{4\sqrt{\left(1-kb-|kc\alpha|\right)}} + \left(\beta^2 - \frac{3}{4}\right)y^2 + \sigma^2 + |e\alpha\beta|\end{aligned} \tag{10}$$

with $0 \le H(x) = -\tanh(0.5|x|) \le 1$

For $\dot{V}(x,y,z) = 0$ and $|kc\alpha| < kb$, a closed polyhedron, M, will exist as:

$$\begin{aligned}&\left(\sqrt{\left(1-kb-|kc\alpha|\right)}x - \frac{\left(\alpha + |d\beta| + I_{ext}\right)}{2\sqrt{\left(1-kb-|kc\alpha|\right)}}\right)^2 - \left(\frac{x}{2}+y\right)^2 + \left(\frac{x}{2}+\beta y\right)^2 + \left(\frac{y}{2}+\sigma\right)^2 \\ &= \frac{\left(\alpha + |d\beta| + I_{ext}\right)^2}{4\sqrt{\left(1-kb-|kc\alpha|\right)}} + \left(\beta^2 - \frac{3}{4}\right)y^2 + \sigma^2 + |e\alpha\beta|\end{aligned} \tag{11}$$

Therefore when $\begin{cases} z \in (L_1, L_2) \\ kb + |kc\alpha| < 1 \end{cases}$, a certain polyhedron m, exist inside of another polyhedron M, such that when (x,y,z) lies at the exterior of m, $\dot{V}(x,y,z) < 0$ and when found at the interior of m, $\dot{V}(x,y,z) > 0$. This reveals that V reaches its highest value on m denoted Ω. Consequently, the set $\{(x,y,z) | V \le \Omega\}$ serves as the ultimate bounded and forward invariant region of the system, ensuring the chaotic trajectories remain restricted within this region.

2.5. Equilibrium points and analysis of their stability

Theoretical studies of the dynamics of the model under investigation are conducted by analyzing its equilibrium points. This is done by setting the left side of relation 5 to 0, from where the following system is obtained:

$$\begin{cases} x^* = -\dfrac{\sigma}{\beta} \\ y^* = \alpha\left(\tanh\left(0.5\left|x^*\right|\right)-1\right)+x^* - I_{ext} - kx^*\left(b+cf\left(z^*\right)\right) \\ f\left(z^*\right) = \dfrac{d}{e}x^* \end{cases} \tag{12}$$

with $I_{ext} = A\sin\left(2\pi ft\right)$.

We observe that the system possesses a fixed state that varies over time, as y^* includes a time-dependent variable influenced by external periodic stimuli I_{ext}.

A linearization of relation 6 around its fixed points as described in Eq. (12), permits us to analyze the stability of the equilibrium points of the system. If $\sigma = 0$, a fixed point is obtained from Eq. (12) as $E = (0, -\alpha - I_{ext}, 0)$, from where the corresponding Jacobian matrix computed at the system's equilibrium state is expressed as:

$$J_E = \begin{pmatrix} -1+kb & 1 & 0 \\ -\beta & 0 & 0 \\ d & 0 & 0 \end{pmatrix} \tag{13}$$

Based on the Jacobian matrix, the characteristic equation is

$$p(\lambda) = \lambda\left[\lambda^2 + (1-kb)\lambda + \beta\right] \tag{14}$$

When $p(\lambda) = 0$, we obtain the three eigenvalues $\lambda_{1,2,3}$ as:

$$\lambda_1 = 0,\ \lambda_{2,3} = \frac{-(1-kb) \pm \sqrt{(1-kb)^2 - 4\beta}}{2} \tag{15}$$

Given that we have one zero eigenvalue and the non-zero eigenvalues are two, the equilibrium point E, can be classified as either unstable or critically stable. The eigenvalues and the related stability of the model for some discrete values of parameter σ are presented in Table 1.

Stability is observed in the system for values of $\sigma < 0$, where both eigenvalues possess negative real parts. Conversely, instability is described in the system for values of $\sigma > 0$, as the eigenvalues have positive real parts.

From these analyses, the enhanced Rulkov neuron model subjected to electromagnetic radiation is seen to be capable of exhibiting hidden and self-excited firings that will respectively originate from its stable and unstable fixed points. Since hidden attractors are generally observed for nonlinear systems with stable fixed points, those with an indefinite number of stationary points and finally, systems with no stationary points [19], and relation 6 is of the second category.

This implies that the improved Rulkov neuron model subjected to electromagnetic radiation will generate hidden or self-excited attractors depending on the value of parameter σ, negative or positive.

3. Numerical investigation of the system's dynamics

The well-known RK4 algorithm is used for the numerical investigations, maintaining a step size of 0.001 throughout each iteration, this paper adopts the values of 1, 0.5 and 0 for the parameters A_m, F_m and N_m that characterizes the internal state function of the memristor. Unless otherwise specified, the starting conditions are set as $(x_0, y_0, z_0) = (0, 0, -0.1)$. The dynamic behaviors of the model are investigated using the same methods exploited in [27-30], such as one-and double-dimensional parameter bifurcation plots, Lyapunov exponents, phase portraits, and time series. The behavior of the model is investigated with the help of some dynamical tools including, 1D and 2D bifurcation diagrams, maximum Lyapunov exponent (MLE), phase portrait and time series.

3.1. Bifurcation analysis

The regions in which the various firing activities of the system are observed are illustrated by computing the two parameter phase diagrams for the planes (A, α), (A, σ) and (α, σ) for which $A \in [-12, 12]$, $\alpha \in [5, 12.5]$ and $\sigma \in [-0.5, 1.5]$. The results obtained are shown in Figure 3, for system parameters taken as $\alpha = 10$, $\beta = 5$, $A = 1$, $f = 1$, $\sigma = 0$, $k = 0.5$, $b = 0.58$, $c = 0.02$, $d = 2.7$ and $e = 1.1$. Two main colors are identified: red for MLE>0 indicating chaotic behaviors and blue for MLE<0 suggesting periodic orbits.

The two parameter charts for the planes (A, σ) and (α, σ) clearly illustrates the regions in which the hidden (for negative values of the parameter σ) and self-excited (for positive values of the parameter σ) attractors of the system are found. Periodic behaviors are characterized by blue color, while chaotic dynamics are described with red color. This result agrees with the analysis carried out on the stability of the model.

The system parameters A, α, β, and f, are individually varied in appropriate ranges to obtain bifurcation diagrams describing the evolution of the system according to each of these parameters. Keeping all other parameter at their original value, the following parameters A,

α, β, and f are adjusted in the intervals $-12 \le A \le 12$, $5 \le \alpha \le 12.5$, $2 \le \beta \le 12$, and $0 \le f \le 1.5$. Figure 4 shows various bifurcation diagrams obtained for each parameter with their corresponding MLE. Figure 4a(i) describes a symmetric and butterfly-shaped bifurcation which occurs with variations in parameter A, where the model transitions from a regular to random behavior, approaching from both directions, right (at -10.5) left (at 10.5) via regular periodic spiking patterns. A slightly similar phenomenon is observed with variations of parameter β shown in Figure 4a(iii). Figure 4a(ii) and 4a(iv) shows a forward and respectively a backward evolution of the system to chaos. The corresponding MLE of each varied parameter is illustrated by Figures 4b(i) to b(iv) and effectively verifies the behaviors of the system with respect to the said parameters.

Considering parameter $A = 1.5$, with all the other parameters unchanged, the Rulkov neuron's chaotic phase portraits when exposed to electromagnetic radiation are obtained as shown in Figure 5.

From Figure 5, one can confirm the complexity of the improved Rulkov neuron model under the electromagnetic induction.

3.2. Offset boosting

Looking closely at relation 6, we can see that y is exclusively present in the model's first equation. Thus, the improved Rulkov neuron model under electromagnetic induction can perform offset boosting features. This is achieved by adjusting the amplitude of the state variable y through the addition of a control parameter as expressed below:

$$\begin{cases} \dot{x} = \alpha\left(-\tanh\left(0.5|x|\right)+1\right) - x + \left(y + B_0\right) + A\sin\left(2\pi ft\right) + kx\left(b + cf\left(z\right)\right) \\ \dot{y} = -\beta x - \sigma \\ \dot{z} = dx - ef\left(z\right) \end{cases} \tag{16}$$

Such a change offers controllable capabilities within the system without hindering in any way its dynamics. The respective bifurcation diagrams of the state variable y in relation to the system parameters A and β are presented in Figures 6a and 6b, for $\alpha = 10$, $A = 1$, $f = 1$, $\sigma = 0$ and $k = 0.5$.

It is noticed that for some discrete values of B_0, the dynamics of the system undergoes a vertical adjustment which can either be positive or negative depending on the value of B_0. Figure 7

further illustrates this as the position of the phase portrait of relation 6 is seen to be adjustable by the control parameter B_0 that causes the state variable y to increase in positive or negative directions depending on whether the value of B_0 is negative or positive respectively.

Figures 8a and 8b respectively illustrates the temporal sequence of the state variable y and the mean values of the state variables x, y and z as a function of the offset boosting parameter B_0. In Figure 8a, y the state variable is adjusted for certain values of the control parameter B_0. From Figure 8b, we remark that only the mean value of y decreases linearly as the offset boosting parameter B_0 takes on increasing negative values, and increases linearly as the parameter rises in positive values. These findings further corroborate the offset boosting features of the system as seen for the bifurcation diagram in Figure 6 and the phase portraits in Figure 7. The offset boosting behavior has been revealed in some HNN models [31-33] and other dynamical systems such as 4D chaotic circuit [34], no equilibrium chaotic circuit [35] and snap chaotic circuit [36].

3.3. Antimonotonicity

This is also called bubble-like bifurcation and refers to the creation followed by the destruction of periodic orbits of a dynamic system [37]. As a result of consecutive period creation and destruction in a nonlinear system, the process of period splitting and its inverse occurs, leading to the emergence of periodic structures in the model. This is disclosed in the model by plotting the local maximum of the state variable x, against the parameters A and β of the system, across specific values of parameter α. The results obtained are shown by Figures 9 and 10.

For remerging Feigenbaum tree, symmetric primary bubbles are obtained when parameter A is used for $\alpha = 7.8$, symmetric period-4 bubbles at $\alpha = 8.5$ and finally, full Feigenbaum remerging tree at $\alpha = 8.8$ and $\alpha = 9.0$ respectively. Similarly, as for the control parameter β, we have a primary bubble for $\alpha = 6.8$, period-4 bubble for $\alpha = 7.4$, period-8 bubble for $\alpha = 7.9$, period-16 bubble for $\alpha = 7.71$ and full Feigenbaum remerging tree for $\alpha = 7.8$, $\alpha = 7.9$ and $\alpha = 8.0$ respectively. In literature, these phenomena have been observed in some neural networks models [38-40] and other systems including the jerk circuits [41] and the improved Colpitts oscillators [42].

4. Microcontroller implementation of the Improved Rulkov neuron under electromagnetic radiation

Following theoretical studies and numerical simulations, it is important to conduct experimental verification, which is essential for many engineering applications [43-45]. One of the most important of these applications is the use of chaotic systems for voice encryption [46]. To verify the validity of the numerically obtained results, which is the main objective of this section, the improved Rulkov neuron model under electromagnetic radiation is practically implemented using an Arduino Due microcontroller. Compared to the implementation of nonlinear dynamical systems using electronic circuits [47-49], this approach has some main advantages such as flexibility in parameters setting of the system, robustness, compactness, re-programmability etc. [50-52]. This implementation utilizes two primary hardware components: The digital card relates to computer and oscilloscope. Various steps followed in view of achieving this implementation are described by the flowchart shown in Figure 11, followed by the experimental setup used in Figure 12.

Relation 5 is resolved by the help of the Runge-Kutta 4th-order (RK4) algorithm in Arduino IDE installed on a laptop computer, from where it is implemented on the Arduino Due board connected to the computer via a programmable USB port and simultaneously, connected to a digital oscilloscope. The attractors showing the route to the chaos obtained from the digital circuit implementation of the model are presented in Figure 13, where we have the numerical results on the left and their corresponding microcontroller implementation counterparts on the right.

The results from Figure 13 show a strong agreement between the numerical and digital circuit implementation findings of the improved Rulkov neuron model under electromagnetic radiation under investigation.

5. Random number generator based on memristive Rulkov neuron model

This section presents an application of the studied memristive Rulkov neuron model in the generation of random numbers. The generated numbers are analyzed using the standard NIST test. The RNG process starts by numerically solving the improved Rulkov neuron model using the RK4 method, which yields high-precision 32-bit state variables x, y, and z signals. To guarantee the high quality and unpredictability required for an RNG, the scheme isolates the Least Significant Bits (LSBs), which are the most sensitive and chaotic part of the numerical solution, by extracting the 16 LSBs from x, y, and z signals. These three streams of

unpredictable binary data are then combined to form the final, statistically robust 32-bit random number sequences suitable for applications like cryptography. To confirm the unpredictable features of the generated signals, the NIST test is done, and results are recorded in Table 2.
The text establishes that to be deemed a high-quality random source; a signal must satisfy the NIST Statistical Test Suite requirement that all P-values for every individual test exceed 0.01. The results from Table 2 demonstrated that all output signals achieved this benchmark, confirming their statistical randomness. Based on these results, the derived random signal from improved Rulkov neuron model is proven reliable and can therefore be utilized effectively in sensitive security applications, such as the encryption necessary for secure information exchange.

6. Conclusion

The impact of the non-polynomial memristor on the dynamic behaviors of the improved Rulkov neuron model was studied in this paper. In the first place, the model's fixed points and stability were explored, revealing that its possesses both critical stable and unstable equilibrium points and in addition to that, displays concealed and self-sustained behaviors featuring both periodic and chaotic bursting patterns for various bifurcation parameter values. This is further confirmed by numerical investigations from where the regions of hidden and self-excited firings are exposed by the two-parameter charts. Secondly, from numerical investigations, the system describes offset boosting and antimonotonicity features. Furthermore, it has been noted that the system undergoes a symmetrical evolution from periodic through spiking firings to chaotic dynamics for some control parameters. To conclude, a model's implementation was done utilizing a digital card. The findings acquired with the aid of a digital oscilloscope show that the experimentally investigated findings corroborate and clearly verify the numerical results. The improved Rulkov neuron was finally exploited to generate random bits and NIST test was performed to confirm the unpredictable features of the generated bits. This system can be further applied in important engineering fields such as medicine and telecommunication for biomedical image and digital signal encryptions respectively.

Author Contributions: Conceptualization, J. T. Tofou; Formal analysis, J. T. Tofou; Funding acquisition, S. Momani; Investigation, V. K. Tamba; Methodology, V. K. Tamba; Supervision,

S. Momani; Visualization, V.-T. Pham; Writing – original draft, J. T. Tofou; Writing – review & editing, V.-T. Pham.

Data Availability Statement: Data is contained within the article.

Conflict of interest: None

Funding: This work is supported by Ajman University Internal Research Grant No. [DRGS Ref. 2024-IRG-HBS-2].

References

[1] Wang Q., Luo R., Wang Y. et al. "Set/Reset Bilaterally Controllable Resistance Switching Ga-doped Ge2Sb2Te5 Long-Term Electronic Synapses for Neuromorphic Computing", Advanced Functional Materials, 33(19), pp. 2213296 (2023). https://doi.org/10.1002/adfm.202213296.

[2] Du G., Zhang H., Yu H., et al. "Study on Automatic Tracking System of Microwave Deicing Device for Railway Contact Wire", IEEE Transactions on Instrumentation and Measurement, 73(2), pp. 1-11 (2024). https://doi.org/10.1109/TIM.2024.3446638.

[3] Ma N., Fang X., Zhang Y., et al. "Enhancing the sensitivity of spin-exchange relaxation-free magnetometers using phase-modulated pump light with external Gaussian noise", Optics Express, 32(19), pp. 33378-33390 (2024). https://doi.org/10.1364/OE.530764.

[4] Hu B., Guo Y., Zhao J., et al. "Possible regulatory mechanisms of typical and atypical absence seizures through an equivalent projection from the subthalamic nucleus to the cortex: Evidence in a computational model", Journal of Theoretical Biology, 112059 pp. 602-603 (2025). https://doi.org/10.1016/j.jtbi.2025.112059.

[5] Cao Y., Ye F., Liang J., et al. "Structural-Functional-Integrated Ultra-Wideband Microwave-Absorbing Composites Based on In Situ-Grown Graphene Meta-nanointerface". Advanced Functional Materials, 34(52), pp. 2411271 (2024). https://doi.org/10.1002/adfm.202411271.

[6] Liang J., Ye F., Song Q., et al. "Genetic algorithm designed multilayered Si3N4 nanowire membranes hybridized by dielectric wide-range tunable CVD graphene skin for broadband microwave absorption", Composites Part B: Engineering, 297, pp. 112298 (2025). https://doi.org/10.1016/j.compositesb.2025.112298.

[7] Tian H., Wang Z., Cao Z., et al. "Field and delay effects on synchronization in a multilayer memristive neuronal network with a hub". Chaos, Solitons and Fractals, 201, pp 117292 (2025). https://doi.org/10.1016/j.chaos.2025.117292.

[8] Lei Y., Dong S., Liang R., et al. "Parallel Resonant Magnetic Field Generator for Biomedical Applications", IEEE Transactions on Biomedical Circuits and Systems, 19(3), pp. 496-510 (2025). https://doi.org/10.1109/TBCAS.2024.3450881.

[9] Chen J., Wang Y., Cui Y., et al. “EEG-based multi-band functional connectivity using corrected amplitude envelope correlation for identifying unfavorable driving states”, Computer Methods in Biomechanics and Biomedical Engineering, pp. 1-13 (2025). https://doi.org/10.1080/10255842.2025.2488502

[10] Wei J., and Lin, H. “Reliability-Oriented Routing of Internal Current Stress in the Two-Stage SST Submodule”, IEEE Transactions on Power Electronics, pp. 1-11 (2025). https://doi.org/10.1109/TPEL.2025.3595961

[11] Cao Y., Chi H., Zhu Z., et al. “Multi-Functional Self-Sensing Electronic Gasket for Structural Health Monitoring of Transportation Pipelines”, Advanced Functional Materials, 35(20), pp. 2412634 (2025). https://doi.org/10.1002/adfm.202412634.

[12] Hodgkin A.L. and Huxley A.F. “A quantitative description of membrane current and its application to conduction and excitation in nerve”, J. Physiol. 117(4) pp. 500-544 (1952). https://doi.org/10.1113/jphysiol.1952.sp004764.

[13] Lin H., Wang C., Deng Q., et al. “Review on chaotic dynamics of memristive neuron and neural network”, Nonlinear Dyn. 106(1) pp. 959-973 (2021). https://doi.org/10.1007/s11071-021-06853-x.

[14] Nagumo J, Arimoto S., and Yoshizawa S. “An active pulse transmission line simulating nerve axon”, Proc. IRE. 50(10) pp. 2061-2070 (1962). https://doi.org/10.1109/JRPROC.1962.288235.

[15] Njitacke Z.T., Nkapkop J. D.D., Signing V.F. et al. “Novel Extreme Multistable Tabu Learning Neuron: Circuit Implementation and Application to Cryptography”, IEEE Trans. Ind. Inform. 19(8) pp. 8943-8952 (2023). https://doi.org/10.1109/TII.2022.3223233.

[16] Rulkov N.F. “Modeling of spiking-bursting neural behavior using two-dimensional map”, Phys. Rev. E, 65(4) pp. 041922 (2002). https://doi.org/10.1103/PhysRevE.65.041922.

[17] Zhang S., Wang C., Zhang H., et al. “A multiplier-free Rulkov neuron under memristive electromagnetic induction: Dynamics analysis, energy calculation, and circuit implementation”, Chaos Interdiscip. J. Nonlinear Sci. 33(8) pp. 083138 (2023). https://doi.org/10.1063/5.0160751.

[18] Xu Q., Liu T., Feng C.T., et al. “Continuous non-autonomous memristive Rulkov model with extreme multistability”, Chin. Phys. B. 30(12) pp. 128702 (2021). https://doi.org/10.1088/1674-1056/ac2f30.

[19] Njitacke Z.T., Takembo C.N., Sani G., et al. “Hidden and self-excited firing activities of an improved Rulkov neuron, and its application in information patterns”, Nonlinear Dyn. 112(15) pp. 13503-13517 (2024). https://doi.org/10.1007/s11071-024-09766-7.

[20] Wan Q., Yan Z., Li F., et al. “Complex dynamics in a Hopfield neural network under electromagnetic induction and electromagnetic radiation”, Chaos Interdiscip. J. Nonlinear Sci. 32(7) pp. 073107 (2022). https://doi.org/10.1063/5.0095384.

[21] Lai Q., and Yang L. “Hyperchaos of neuron under local active discrete memristor simulating electromagnetic radiation”, Chaos 34, pp. 013145 (2024). https://doi.org/10.1063/5.0182723.

[22] Xu Q., Liu T., Ding S., et al. “Extreme multistability and phase synchronization in a heterogeneous bi-neuron Rulkov network with memristive electromagnetic induction”, Cognitive Neurodynamics 17, pp. 755-766 (2023). https://doi.org/10.1007/s11571-022-09866-3.

[23] Li K., Bao H, Li H., et al. “Memristive Rulkov neuron model with magnetic induction effects”, IEEE Transactions on Industrial Informatics, 18(3) pp. 1726-1736 (2022). https://doi.org/10.1109/TII.2021.3086819.

[24] Dawei D., Yan N., Zongli Y., et al. “Extreme multi-stability and microchaos of fractional-order memristive Rulkov neuron model considering magnetic induction and its digital watermarking application”, Nonlinear Dynamics 112(17), pp. 1-23 (2024). https://doi.org/10.1007/s11071-024-09610-y.

[25] Lv M., Wang C., Ren G., et al. “Model of electrical activity in a neuron under magnetic flow effect”, Nonlinear Dyn. 85(3), pp. 1479-1490 (2016). https://doi.org/10.1007/s11071-016-2773-6.

[26] Yu F., Kong X. Yao W., et al. “Dynamics analysis, synchronization and FPGA implementation of multiscroll Hopfield neural networks with non-polynomial memristor”, Chaos Solitons Fractals 179, pp. 114440 (2024). https://doi.org/10.1016/j.chaos.2023.114440.

[27] Ding X., Fan W., Wang N., et al. “Dynamical behaviors and firing patterns in a fully memory-element emulator-based bionic circuit”, Chaos, Solitons and Fractals 199(1), pp. 0960-0779 (2025). https://doi.org/10.1016/j.chaos.2025.116658.

[28] Mehrabbeik M., Jafari S., Sprott J.C., “A simple three-dimensional quadratic flow with an attracting torus”, Physics Letters A 451, pp. 0375-9601 (2022). https://doi.org/10.1016/j.physleta.2022.128427.

[29] Veeman D., Mehrabbeik M., Natiq H., et al. “A New Chaotic System with Coexisting Attractors”, International Journal of Bifurcation and Chaos 32(3), pp. 2230007 (2022). https://doi.org/10.1142/S0218127422300075.

[30] Barathi G., Natiq H., He S., et al. “A A Novel Dynamical System: Chaos, Hidden Dynamics, Multistability, and Applications”, International Journal of Bifurcation and Chaos 35(7), pp. 2530015 (2025). https://doi.org/10.1142/S0218127425300150.

[31] Leng X., Wang X., Zeng Z. “Memristive Hopfield neural network with multiple controllable nonlinear offset behaviors and its medical encryption application”, Chaos, Solitons and Fractals 183, pp. 114944 (2024). https://doi.org/10.1016/j.chaos.2024.114944.

[32] Bao H., Hua M., Ma J., et al. “Offset-control plane coexisting behaviors in two-memristor-based Hopfield neural network”, IEEE Transactions on Industrial Electronics 70(10) pp. 10526-10535 (2023). https://doi.org/10.1109/TIE.2022.3222607.

[33] Lin H, Wang C., Yu F., et al. “A triple-memristor Hopfield neural network with space multistructure attractors and space initial-offset behaviors”, IEEE Transactions on Computer-Aided Design of Integrated Circuits and Systems 42(12), pp. 4948-4958 (2023). https://doi.org/10.1109/TCAD.2023.3287760.

[34] Kamdoum Tamba V., Kom G.H., Kingni S.T., et al. “Analysis and electronic circuit implementation of an integer- and fractional-order four-dimensional chaotic system with offset boosting and hidden attractors”, Eur. Phys. J. Spec. Top. 229, pp. 1211-1230 (2020). https://doi.org/10.1140/epjst/e2020-900169-1.

[35] Mboupda Pone J.R., Kamdoum Tamba V., Kom G.H., et al. “Numerical, electronic simulations and experimental analysis of a no-equilibrium point chaotic circuit with offset boosting and partial amplitude control”, SN Appl. Sci. 1, pp. 922 (2019). https://doi.org/10.1007/s42452-019-0956-8.

[36] Takougang Tchinda S.F., Mpame G., Nzeukou Takougang A.C., et al. “Dynamic analysis of a snap oscillator based on a unique diode nonlinearity effect, offset boosting control and sliding mode control design for global chaos synchronization”, J. Control. Autom. Electr. Syst. 30, pp. 970-984 (2019). https://doi.org/10.1007/s40313-019-00518-2.

[37] Dawson S.P., Grebogi C., Yorke J.A., et al. “Antimonotonicity: inevitable reversals of period-doubling cascades”, Phys Lett A 62, pp. 249-254 (1992). https://doi.org/10.1016/0375-9601(92)90442-O.

[38] Zhang X., Min F., Dou Y., Xuy. “Bifurcation analysis of a modified FitzHugh-Nagumo neuron with electric field”, Chaos, Solitons and Fractals 170, pp. 113415 (2023). https://doi.org/10.1016/j.chaos.2023.113415.

[39] Mbanda Biamou A.L., Kamdoum Tamba V., Kapche Tagne F., et al. “Fractional-order-induced symmetric multi-scroll chaotic attractors and double bubble bifurcations in a memristive coupled Hopfield neural networks”, Chaos, Solitons and Fractals 178 pp. 114267 (2024). https://doi.org/10.1016/j.chaos.2023.114267.

[40] Kamdoum Tamba V., Mbanda Biamou A.L., Pham V.T., et al. “Fractional-order bi-Hopfield neuron coupled via a multistable memristor: Complex neuronal dynamic analysis and implementation with microcontroller”, Int. J. Electron. Commun. 191, pp. 155661 (2025). https://doi.org/10.1016/j.aeue.2025.155661.

[41] Kengne J., Mogue R.L.T., Fozin T.F., et al. “Effects of symmetric and asymmetric nonlinearity on the dynamics of a novel chaotic jerk circuit: Coexisting multiple attractors, period doubling reversals, crisis, and offset boosting”, Chaos Solitons Fractals 121, pp. 63-84 (2019). https://doi.org/10.1016/j.chaos.2019.01.033.

[42] Kamdoum Tamba V., Fotsin H.B., Kengne J., et al. "Emergence of complex dynamical behaviors in improved Colpitts oscillators: antimonotonicity, coexisting attractors, and metastable chaos", Int. J. Dyn. Control. 5(3), pp. 395-406 (2017). https://doi.org/10.1007/s40435-016-0223-4.

[43] Liu X., Zhao L., and Jin J. "A noise-tolerant fuzzy-type zeroing neural network for robust synchronization of chaotic systems", Concurrency and Computation: Practice and Experience 36(22), pp. e8218 (2024). doi: https://doi.org/10.1002/cpe.8218

[44] Guo X., Zhang J., Meng X., et al. "HALTRAV: Design of a High-Performance and Area-Efficient Latch With Triple-Node-Upset Recovery and Algorithm-Based Verifications", IEEE Transactions on Computer-Aided Design of Integrated Circuits and Systems, 44(6), pp. 2367-2377 (2025). https://doi.org/10.1109/TCAD.2024.3511335

[45] Zhang T., Hu H., Jiang H., et al. "KNN-based frequency-adjustable ferroelectric heterojunction and biomedical applications", Nature Communications, 16(1), pp. 7120 (2025). https://doi.org/10.1038/s41467-025-62079-0.

[46] Li Z., Jin J., Zhang D., et al. "An attractor-controllable memristive Hopfield neural network and its application on voice encryption", Integration, 105, pp. 102500 (2025). https://doi.org/10.1016/j.vlsi.2025.102500.

[47] Chong Z., Wang C., Zhang H., et al. "Sine-Transform-Based Dual-Memristor Hyperchaotic Map and Analog Circuit Implementation". IEEE Transactions on Instrumentation and Measurement, 74, pp. 1-14 (2025). https://doi.org/10.1109/TIM.2025.3570347.

[48] Dong S., Huang Q., Luo H., et al. "A Design and Analysis of RCD Oscillation Suppression Circuit for Marx Pulse Generator", IEEE Transactions on Plasma Science, 53(6), pp. 1277-1284 (2025). https://doi.org/10.1109/TPS.2025.3559507

[49] Tian H., Yi X., Zhang Y., et al. "Dynamical Analysis, Feedback Control Circuit Implementation, and Fixed-Time Sliding Mode Synchronization of a Novel 4D Chaotic System", Symmetry, 17(8), pp. 1252 (2025). https://doi.org/10.3390/sym17081252

[50] Kose E. and Muhurcu A. "Realization of a digital chaotic oscillator by using a low cost microcontroller", Engineering Review 37, pp. 341-348 (2017).

[51] Wu E., Wang Y., Huo S., et al. "Universal Core–Shell Nanowire Memristor Platform with Quasi-2D Filament Confinement for Scalable Neuromorphic Applications", Advanced Functional Materials, e18764 (2025). https://doi.org/10.1002/adfm.202518764.

[52] Wang C., Chong Z., Zhang H., et al. "Color image encryption based on discrete memristor logistic map and DNA encoding", Integration 96, pp. 102138 (2024). https://doi.org/10.1016/j.vlsi.2024.102138.

Biographies :

Victor Kamdoum Tamba received his PhD degree in Physics, specialty Electronics, from the University of Dschang (Cameroon). He is a senior Lecturer/Researcher in the same University. His scientific research interests include nonlinear systems/circuits, chaos, analog/digital system implementations, chaos synchronization with related applications in engineering. He is co-author of more than 75 scientific publications. He serves as reviewer for renowned international journals including, Chaos an Interdisciplinary Journal of Nonlinear Science, Nonlinear Dynamics, Chaos Solitons and Fractals, IEEE Transactions and Cybernetics, IEEE Transactions on Industrial Informatics, IEEE Transactions on Systems, Man and Cybernetics, IEEE Internet of Thing, IEEE Access.

Junior Tchiaze Tofou received his master degree in Physics, specialty Electronics, from the University of Dschang (Cameroon). He is currently a PhD student in the same University. His scientific research interests include dynamical chaotic systems and their application to communication systems.

Prof. Shaher Momani received his B.Sc. in Mathematics from Yarmouk University in 1984 and his PhD from the University of Wales, Aberystwyth, in 1991 under the supervision of Prof. Ken Walters, FRS. He has held academic positions at Mutah University, Yarmouk University, United Arab Emirates University, Qatar University, and has been a Professor at The University of Jordan since 2009, while serving as a Distinguished Professor at Ajman University (2019-present). A leading researcher in fractional calculus, Prof. Momani has published over 500 scientific papers and has been ranked among the world's top ten scientists in this field since 2009.

Viet-Thanh Pham received the PhD degree in electronics, automation and control of complex systems engineering from the University of Catania. He is working for the Industrial University of Ho Chi Minh City. His scientific research interests include chaos, nonlinear control, fractional-order systems, mathematical modelling, machine learning, and applications of nonlinear systems.

Figure captions

Figure 1: Memristor's features. (a) I-V characteristics versus A, (b) I-V characteristics versus f, and (c) its power-off plot. Parameter's values are $b=0.58$, $c=0.02$, $d=2.7$, $e=1.1$ and $x(0)=3$.

Figure 2: Topology illustration of the improved Rulkov neuron subjected to electromagnetic radiation mimic by a non-polynomial memristor.

Figure 3: Dual-parameters bifurcation diagrams of Rulkov neuron model. (a) $(A,\ \alpha)$ for $\beta=5$ and $\sigma=0$, (b) $(A,\ \sigma)$ for $\alpha=10$ and $\beta=5$ and (c) $(\alpha,\ \sigma)$ for $\beta=5$ and $A=1$. Other parameter's values are: $f=1$ and $k=0.5$.

Figure 4: Varieties of 1D bifurcation diagrams a(i)-a(iv) with corresponding MLE b(i)-b(iv) of Rulkov neuron model versus A, α, β, and f. Other parameters are kept to their initial values as fixed in Fig. 3.

Figure 5: Projected phase portraits of Rulkov neuron model in some of its planes. Parameter's values are $\alpha=10$, $\beta=5$, $A=1.5$, $f=1$, $\sigma=0$ and $k=0.5$.

Figure 6: Adaptation of the amplification of Rulkov neuron model when (a) $A \in [0,\ 12]$ and (b) $\beta \in [0,\ 12]$ for some discrete values of B_0 indicated on the graph. Other parameters are kept to their initial values as fixed in Fig. 3.

Figure 7: Phase portraits illustrating the offset boosting behaviors in Rulkov neuron model computed from left to right with $B_0 = -5$, $B_0 = 0$, and $B_0 = 5$, respectively. The other system parameters maintained at their initial values.

Figure 8: Temporal sequences of the state variable y (a) and mean values of the state variables x, y and z versus B_0 (b), confirming the offset boosting behaviors in Rulkov neuron model. They are plotted for $B_0 = -5$ (black), $B_0 = 0$ (magenta) and $B_0 = 5$ (red).

Figure 9: Bifurcation diagrams versus A, revealing bubble behaviors in Rulkov neuron model for some specific values of α. (a) α =7.8 ; (b) α =8.5 ; (c) α =8.8 ; and (d) α =9.

Figure 10: Bifurcation diagrams versus β, revealing bubble behaviors in Rulkov neuron model for some specific values of α. (a) α =6.8 ; (b) α =7.4 ; (c) α =7.65 ; (d) α =7.71; (e) α =7.8; (f) α =7.9; and (g) α =8.

Figure 11: Flowchart diagram describing the key steps of the microprocessor implementation process of Rulkov neuron model under the electromagnetic induction.

Figure 12: Experimental setup showing the main hardware components including oscilloscope and Arduino Due microcontroller board with some connecting cables.

Figure 13: Numerical (left) and experimental (right) phase of Rulkov neuron model. (a) $A = 10.22$ (period-1 limit cycle), (b) $A = 7.92$ (period-2 limit cycle), (c) $A = 5.40$ (period-3 limit cycle), (d) $A = 4.92$ (period-6), (e) $A = 4.56$ (chaos), and (f) $A = 3.36$ (chaos).

List of Tables

Table 1 : Eigenvalues and their associated stability for particular values of the parameter σ for $\beta = 5$, $k = 0.5$ and $b = 0.58$.

Table 2: RNG of NIST-800-22 tests for x, y and z output signals

List of Figures

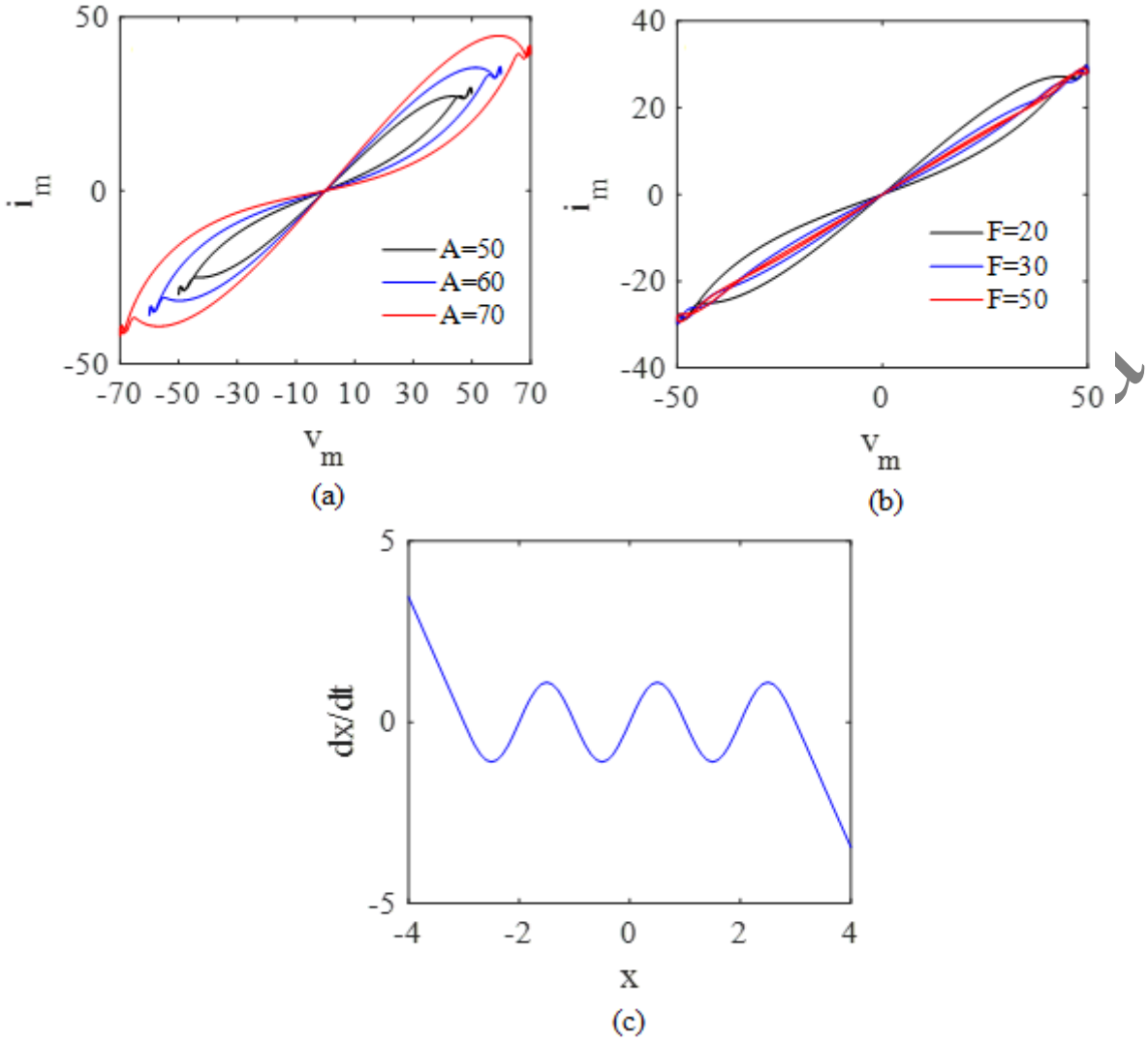

Figure 1: Memristor's features: (a) I-V characteristics versus A, (b) I-V characteristics versus f, and (c) its power-off plot. Parameter's values are $b=0.58$, $c=0.02$, $d=2.7$, $e=1.1$ and $x(0)=3$.

Figure 2: Topology illustration of the improved Rulkov neuron subjected to electromagnetic radiation mimic by a non-polynomial memristor.

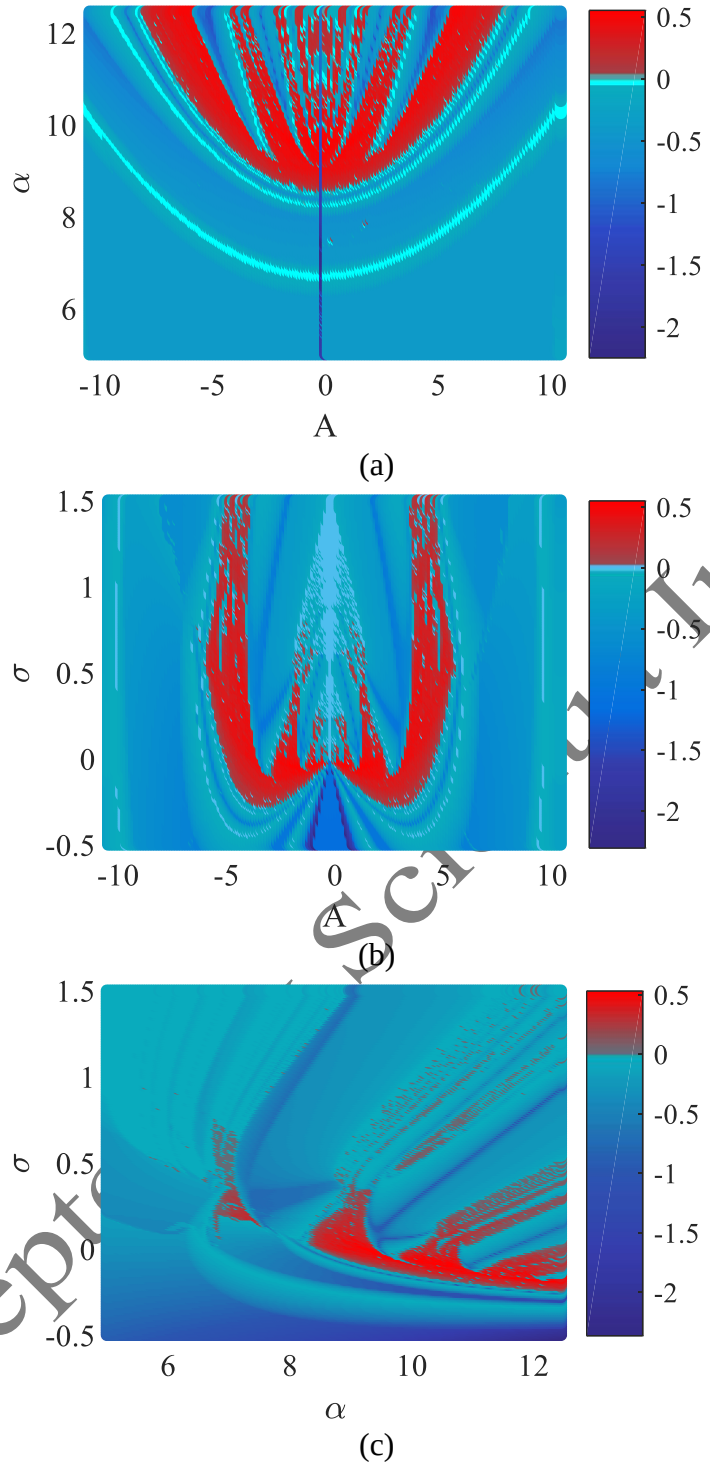

Figure 3: Dual-parameters bifurcation diagrams of Rulkov neuron model. (a) $(A,\ \alpha)$ for $\beta=5$ and $\sigma=0$, (b) $(A,\ \sigma)$ for $\alpha=10$ and $\beta=5$ and (c) $(\alpha,\ \sigma)$ for $\beta=5$ and $A=1$. Other parameter's values are: $f=1$ and $k=0.5$.

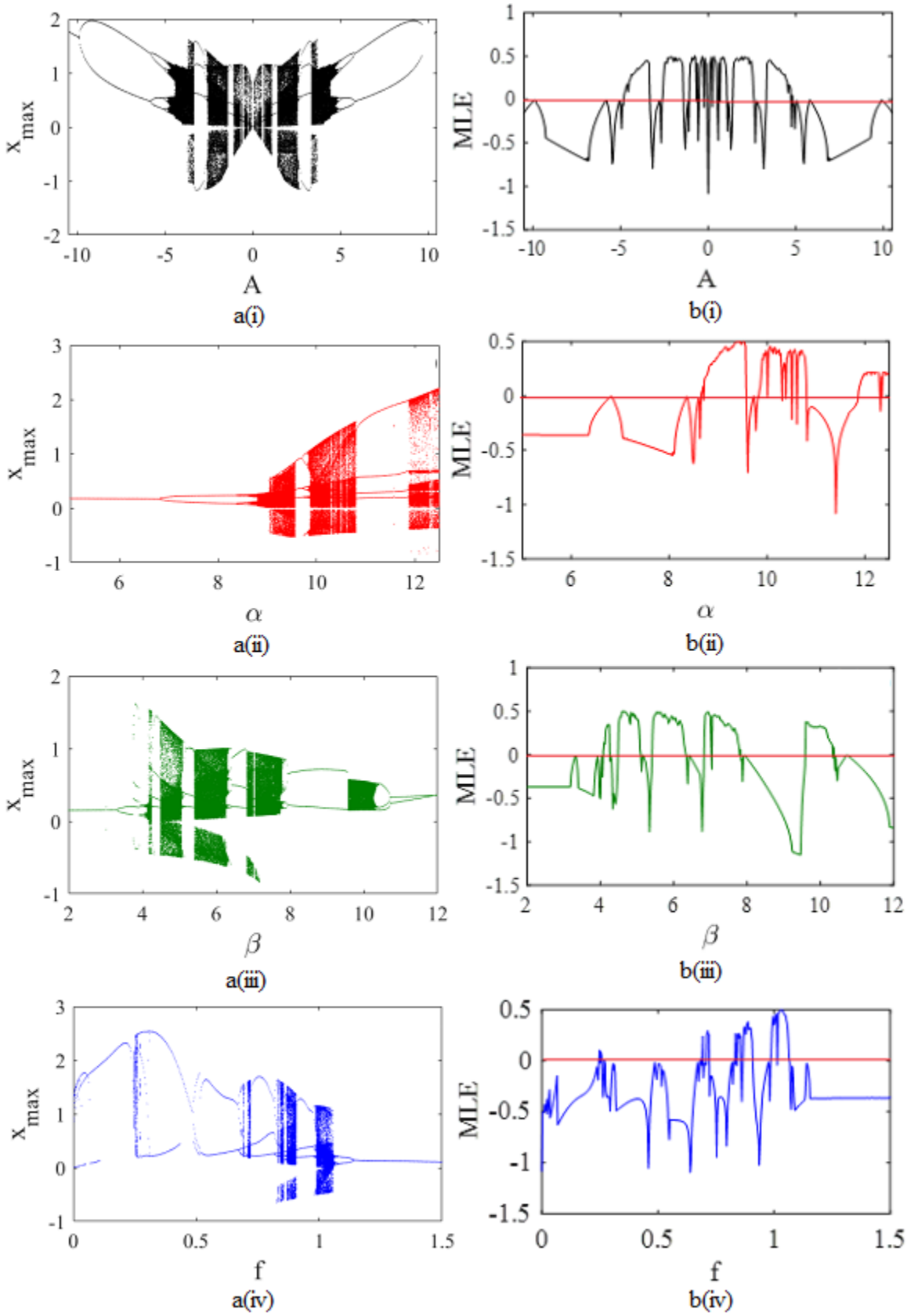

Figure 4: Varieties of 1D bifurcation diagrams a(i)-a(iv) with corresponding MLE b(i)-b(iv) of Rulkov neuron model versus A, α, β, and f. Other parameters are kept to their initial values as fixed in Fig. 3.

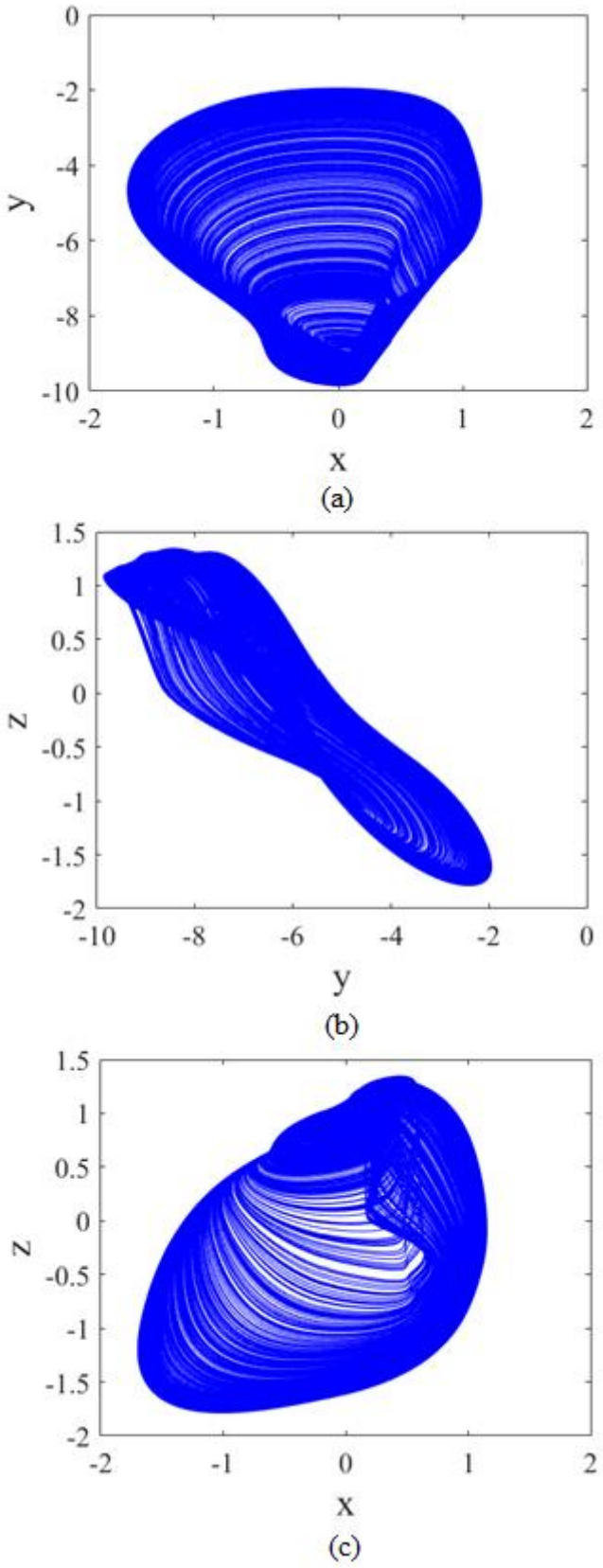

Figure 5: Projected phase portraits of Rulkov neuron model in some of its planes. Parameter's values are $\alpha = 10$, $\beta = 5$, $A = 1.5$, $f = 1$, $\sigma = 0$ and $k = 0.5$.

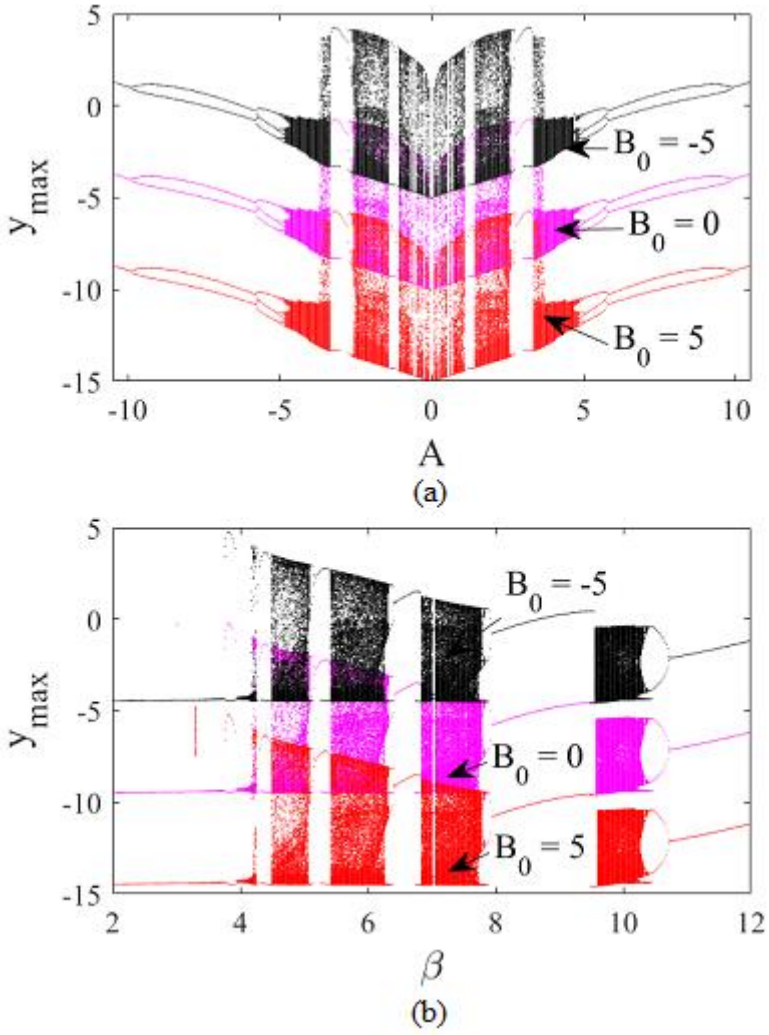

Figure 6: Adaptation of the amplification of Rulkov neuron model when (a) $A \in [0,\ 12]$ and (b) $\beta \in [0,\ 12]$ for some discrete values of B_0 indicated on the graph. Other parameters are kept to their initial values as fixed in Fig. 3.

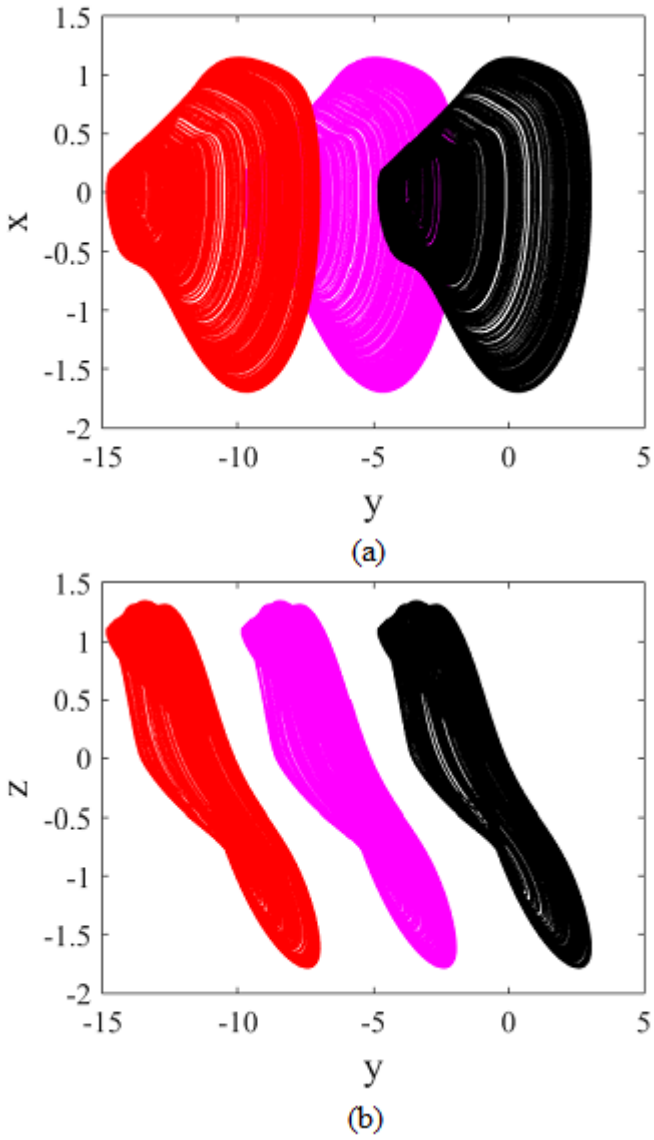

Figure 7: Phase portraits illustrating the offset boosting behaviors in Rulkov neuron model computed from left to right with $B_0 = -5$, $B_0 = 0$, and $B_0 = 5$, respectively. The other system parameters maintained at their initial values.

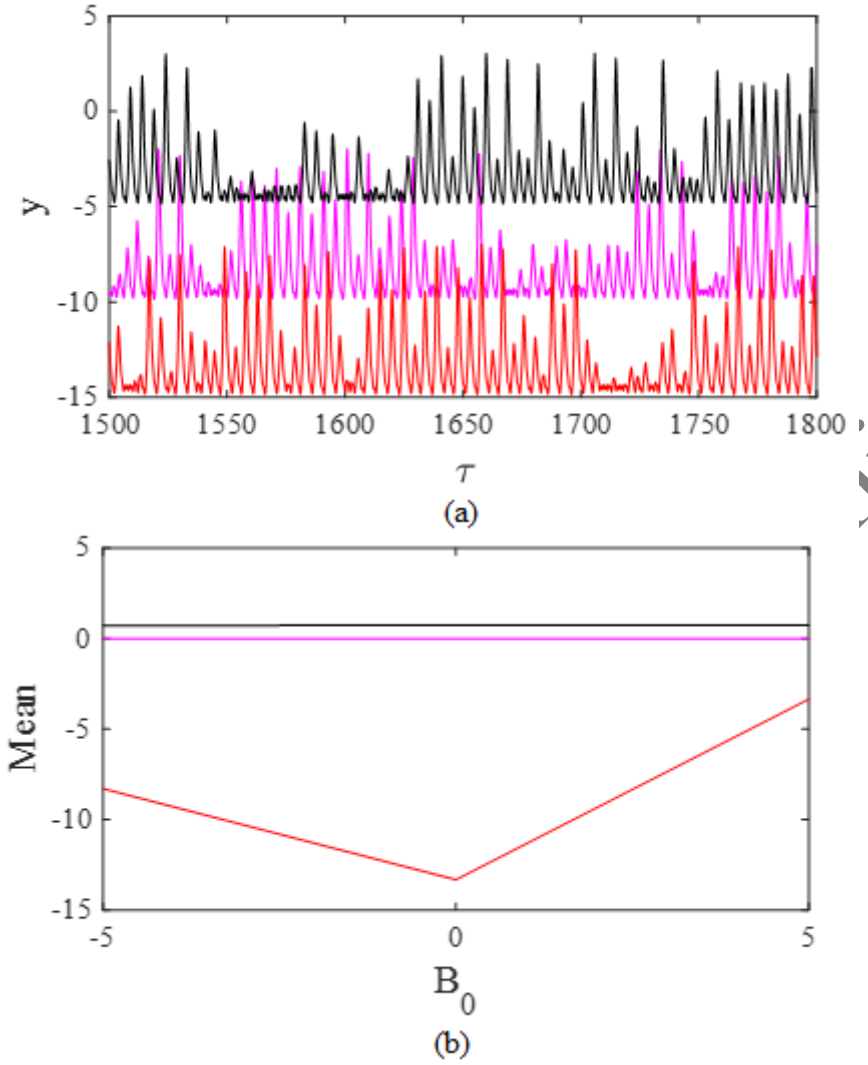

Figure 8: Temporal sequences of the state variable y (a) and mean values of the state variables x, y and z versus B_0 (b), confirming the offset boosting behaviors in Rulkov neuron model. They are plotted for $B_0 = -5$ (black), $B_0 = 0$ (magenta) and $B_0 = 5$ (red).

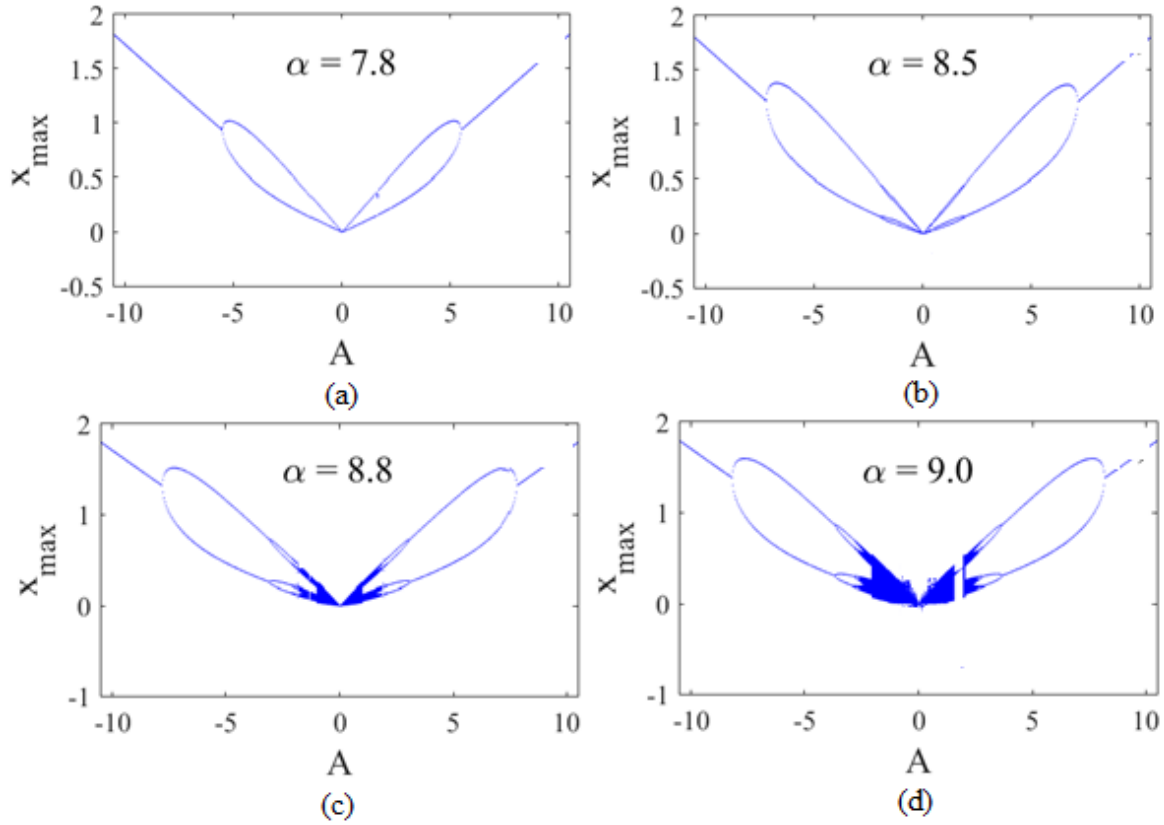

Figure 9: Bifurcation diagrams versus A, revealing bubble behaviors in Rulkov neuron model for some specific values of α . (a) α =7.8 ; (b) α =8.5 ; (c) α =8.8 ; and (d) α =9.

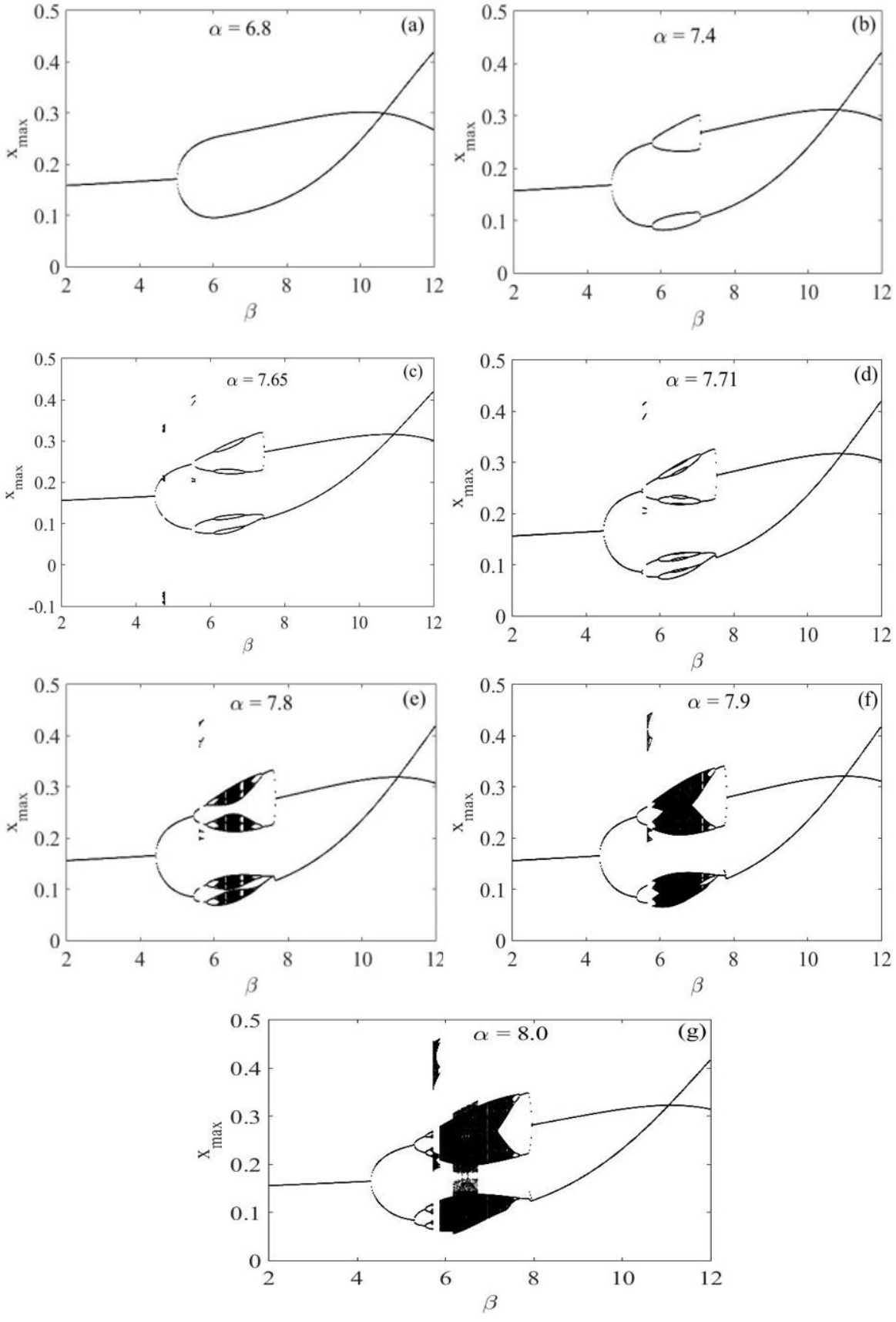
α = 6.8
(a)
α = 7.4
(b)
α = 7.65
(c)
α = 7.71
(d)
α = 7.8
(e)
α = 7.9
(f)
α = 8.0
(g)
x_max
β

Figure 10: Bifurcation diagrams versus β , revealing bubble behaviors in Rulkov neuron model for some specific values of α . (a) α =6.8 ; (b) α =7.4 ; (c) α =7.65 ; (d) α =7.71; (e) α =7.8; (f) α =7.9; and (g) α =8.

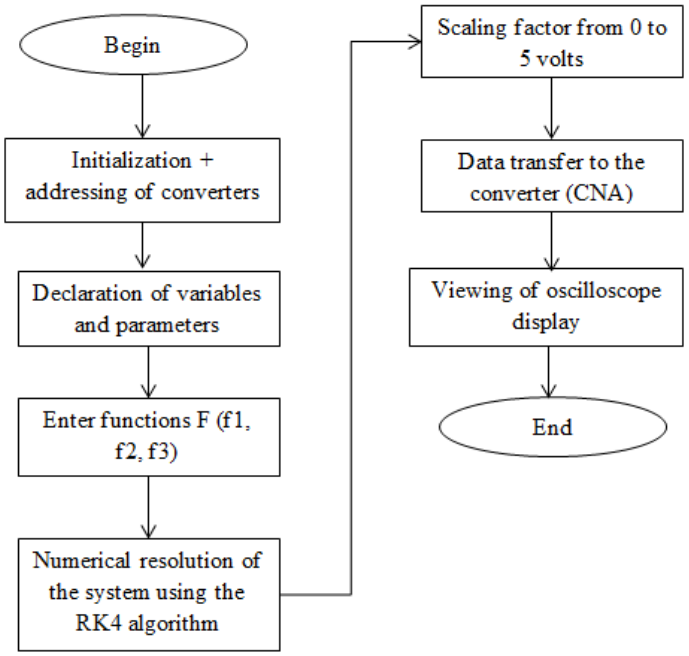

Figure 11: Flowchart diagram describing the key steps of the microprocessor implementation process of Rulkov neuron model under the electromagnetic induction.

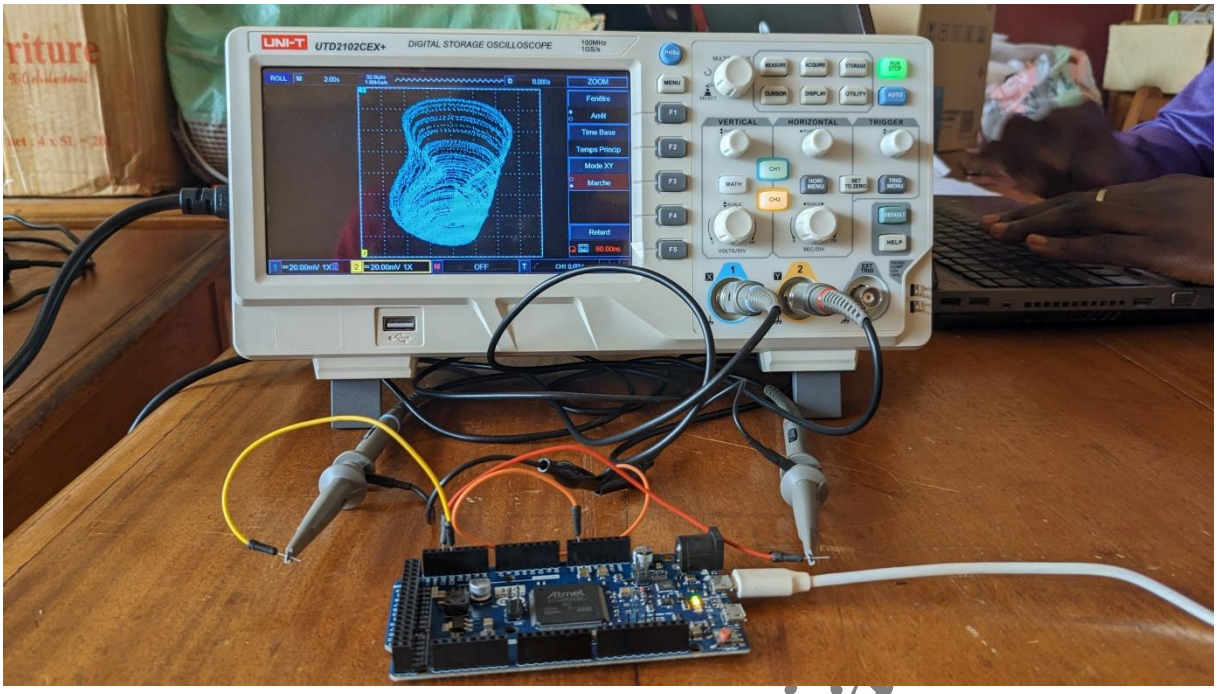

Figure 12: Experimental setup showing the main hardware components including oscilloscope and Arduino Due microcontroller board with some connecting cables.

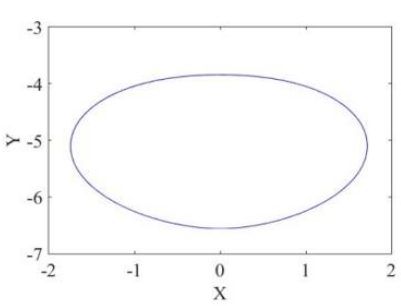

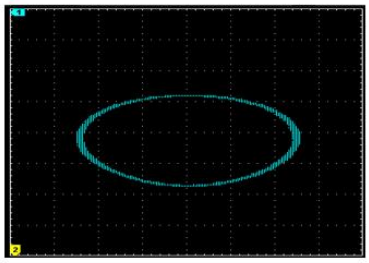

(a)

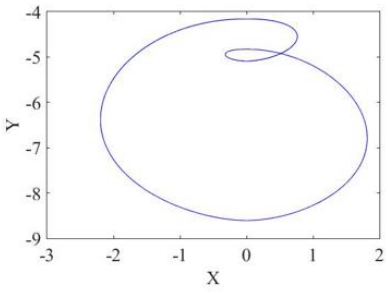

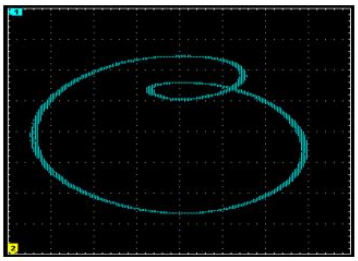

(b)

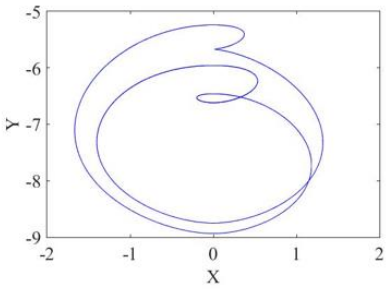

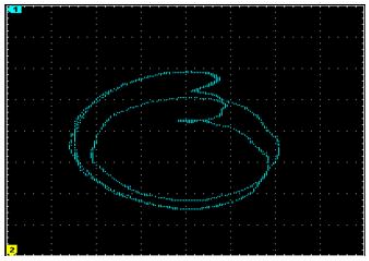

(c)

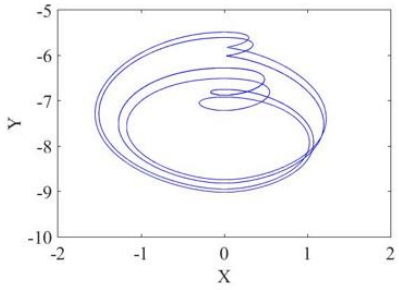

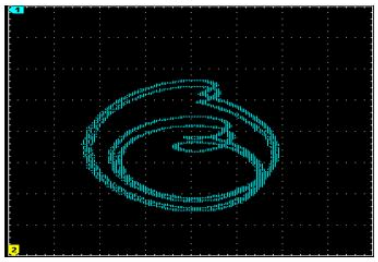

(d)

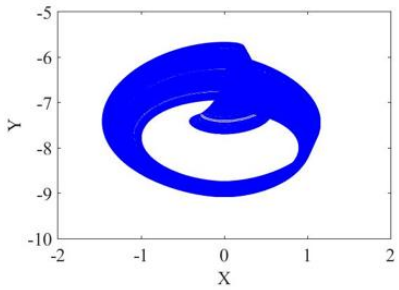

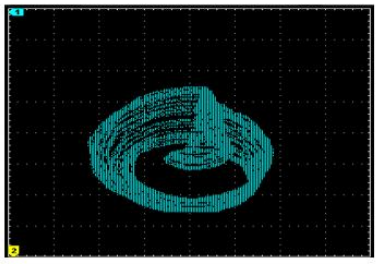

(e)

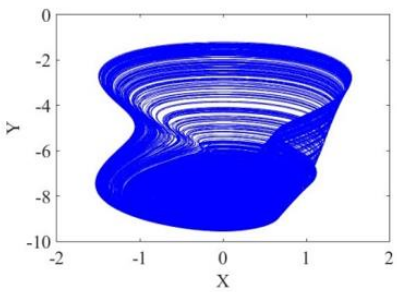

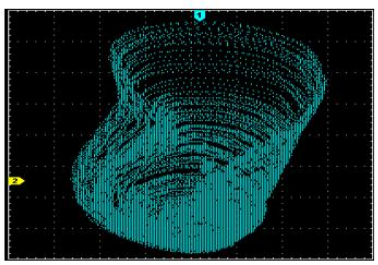

(f)

Figure 13: Numerical (left) and experimental (right) phase of Rulkov neuron model. (a) $A=10.22$ (period-1 limit cycle), (b) $A=7.92$ (period-2 limit cycle), (c) $A=5.40$ (period-3 limit cycle), (d) $A=4.92$ (period-6), (e) $A=4.56$ (chaos), and (f) $A=3.36$ (chaos).

List of Tables

Table 2 : Eigenvalues and their associated stability for particular values of the parameter σ for $\beta=5$, $k=0.5$ and $b=0.58$.

σ	Eigenvalues $(\lambda_{2,3})$	Stability
-1.5	$-1.1180,\ -4.4723$	Critical stable
-1	$-1.0972,\ -4.5572$	Critical stable
-0.5	$-1.0846,\ -4.6099$	Critical stable
0	$-0.3550\pm 2.2077i$	Critical stable
0.5	$2.1373\pm 0.6573i$	Unstable
1	$2.1172\pm 0.7194i$	Unstable
1.5	$2.0851\pm 0.8076i$	Unstable

Table 2: RNG of NIST-800-22 tests for x, y and z output signals

Test-Name	P-value (x)	P-value (y)	P-value (z)	Results
Frequency	0.38430	0.63265	0,81318	successful
Block-frequency	0.45659	0.85907	0,06568	successful
Runs	0.64497	0.40104	0,57507	successful
Longest runs of ones	0.38017	0.84658	0,08665	successful
Rank	0.97309	0.54907	0,14108	successful
DFT	0.54474	0.12315	0,05560	successful
No overlapping templates	0.40342	0.01843	0,00371	successful
Overlapping templates	0.25315	0.86426	0,88328	successful
Universal	0.47963	0.89316	0,30245	successful
Linear complexity	0.36285	0.36634	0,58439	successful
Serial test 1	0.58486	0.58636	0,83715	successful
Serial test 2	0.62531	0.67638	0,20581	successful
Approximate entropy	0.24149	0.04793	0,63419	successful
Cumulative sums (forward)	0.72614	0.73365	0,99067	successful
Random excursions x= 4	0.92159	0.73991	0,45278	successful
Random excursions variant x= 1	0.73946	0.51414	0,75399	successful